Published in final edited form as:
Dev Biol. 2011 August 15; 356(2): 432–444. doi:10.1016/j.ydbio.2011.05.667.

Muscles in a mouse model of spinal muscular atrophy show profound defects in neuromuscular development even in the absence of failure in neuromuscular transmission or loss of motor neurons

Young il Lee[1], **Michelle Mikesh**[1], **Ian Smith**[1], **Mendell Rimer**[2], and **Wesley Thompson**[1]

[1]Section of Molecular Cell and Developmental Biology, The University of Texas, Austin, TX 78712

[2]Dept. of Neuroscience and Experimental Therapeutics, College of Medicine, Texas A&M Health Science Center, College Station, TX 77843

Abstract

A mouse model of the devastating human disease "spinal muscular atrophy" (SMA) was used to investigate the severe muscle weakness and spasticity that precedes the death of these animals near the end of the 2nd postnatal week. Counts of motor units to the soleus muscle as well as of axons in the soleus muscle nerve showed no loss of motor neurons. Similarly, neither immunostaining of neuromuscular junctions nor the measurement of the tension generated by nerve stimulation gave evidence of any significant impairment in neuromuscular transmission, even when animals were maintained up to 5 days longer via a supplementary diet. However, the muscles were clearly weaker, generating less than half their normal tension. Weakness in 3 muscles examined in the study appears due to a severe but uniform reduction in muscle fiber size. The size reduction results from a failure of muscle fibers to grow during early postnatal development and, in soleus, to a reduction in number of fibers generated. Neuromuscular development is severely delayed in these mutant animals: expression of myosin heavy chain isoforms, the elimination of polyneuronal innervation, the maturation in the shape of the AChR plaque, the arrival of SCs at the junctions and their coverage of the nerve terminal, the development of junctional folds. Thus, if SMA in this particular mouse is a disease of motor neurons, it can act in a manner that does not result in their death or disconnection from their targets but nonetheless alters many aspects of neuromuscular development.

Keywords

Spinal muscular atrophy; neuromuscular junction; Schwann cells; skeletal muscle development; mouse model

Corresponding authors: Young il Lee, Ph.D., Section of Molecular Cell and Developmental Biology, The University of Texas, Austin, TX 78712, youngil.lee@mail.utexas.edu, Wesley Thompson, Ph.D., Section of Molecular Cell and Developmental Biology, The University of Texas, Austin, TX 78712, wes@mail.utexas.edu.

Introduction

Spinal muscular atrophy (SMA) is a genetic disease characterized by muscle weakness that varies in severity and age of onset (Crawford and Pardo, 1996; Monani, 2005). It is widely believed to be caused by defects in spinal motor neurons. Severe forms of SMA are fatal and constitute the leading genetic cause of mortality in infants. The genetics of this complex disease is now well understood. All human patients with SMA carry mutations in or deletion of both copies of a telomeric gene "*survival of motor neuron 1*" or "*SMN1*" that codes for a protein "SMN" that, surprisingly, is present in all cells in the body and is believed to be involved in RNA processing (Burghes and Beattie, 2009; Lefebvre et al., 1995). Loss of all SMN results in embryonic lethality. However, due to gene duplication, humans possess another centromeric gene, *SMN2*, that is identical to *SMN1* save for a silent mutation that results in inefficient splicing leading to a truncated protein (SMNΔ7). SMNΔ7 is unstable and unable to compensate for the loss of *smn1* (Lorson and Androphy, 2000). Full length SMN is produced at only ~10% of the level encoded by *SMN1* (Lorson et al., 1999). The severity and onset of the disease in humans depend on the number of copies of *SMN2* present (Parsons et al., 1998). Thus, human patients have a reduction in, rather than a loss of, SMN. A central issue has been which tissues are most susceptible to this reduction and lead to muscle weakness.

To investigate the disease, mouse models have been generated (for review see Park et al., 2010a). Since mice possess only a single *smn* gene, the loss of which is embryonic lethal, transgenes to mimic the second locus present in humans have been introduced into the *smn* null background. For example, introduction of copies of the human *SMN2* gene and a transgene derived from the cDNA of SMNΔ7 yields mice (termed SMAΔ7 mice) that display gross motor defects, fail to thrive, and die near P16 (postnatal day 16) (Le et al., 2005). Studies have been conducted on these mice in attempt to characterize the nature of the defects both physiologically and morphologically. The results of these studies have been rather divided as to the motor neuron selectivity of the phenotype (for example Kariya et al., 2008; Ling et al., 2010) – is SMA a motor neuron disease in which SMN deficiency causes death selectively of motor neurons, leading subsequently to muscle atrophy? Attempts at tissue-specific rescue of SMN expression in these (or similar mouse models) suggest motor neuron involvement but the importance of reduced SMN expression in other tissues has not been ruled out (Azzouz et al., 2004; Gavrilina et al., 2008). Here we report our attempts to characterize the SMNΔ7 mice. Our findings suggest that muscle weakness is associated with a slowed neuromuscular development that occurs in all 3 muscles we examined but is not associated with motor neuron death or loss of effective innervation of muscle fibers. These results suggest that alterations in morphology and behavior of multiple cell types of the neuromuscular system affect the progress of the disease and that neuromuscular activity rather than motor innervation per se plays a role in the disease phenotype.

Materials and Methods

Animals

Animal care and experiments were conducted in accordance with National Institutes of Health guidelines and were approved by the University of Texas Institutional Animal Care and Use Committee. The SMAΔ7 mice were acquired from Jackson Labs (stock number 005025) with the assistance of the Spinal Muscular Atrophy Foundation. These mice, originally generated in the laboratory of Arthur Burgess (Le et al., 2005) are homozygous for each of two transgenes (h*SMN*2 and *SMNΔ7*) that allow mice that are homozgyous null for mouse *smn* and would otherwise die embryonically to survive to the end of the second postnatal week. To maintain this colony required only identifying mice heterozygous for deletion of *smn*, mice that are fully viable. This was done by PCR for the detection of wild

type and knockout *smn* alleles, using primers previously described (Schrank et al., 1997). Mice afflicted with SMA (i.e. those homozygous mutant for *smn*; *smn* −/−) were identified in the progeny of heterozygous mating stock. These mice could be easily identified by P5 based on deficits in ambulatory and righting behavior as well as their small size, as described previously (Le et al., 2005). This identification could be confirmed by genotyping using PCR. Animals examined in this study were euthanized by intraperitoneal injections of Nembutal (200 mg/kg).

To facilitate fluorescence imaging of terminal Schwann cells (tSC), an S100-eGFP transgene that marks SCs by their cytoplasmic expression of enhanced green fluorescent protein (Kang et al., 2003; Zuo et al., 2004) was introduced into the SMAΔ7 line by interbreeding. The offspring were successively backcrossed to SMAΔ7 mice to place the S100-eGFP transgene in the FVB background of the original SMA line. Mice with the S100-eGFP transgene were identified visually by GFP fluorescence present in the lens of their eye or by PCR (Zuo et al., 2004). Mice hemizygous for the deletion of the mouse *smn* gene were identified by PCR as described above. Mice homozygous for the two original transgenes in this line (*hSMN2* and *SMNΔ7*) were identified by quantitative PCR using reagents designed by Mary Ann Mann and performed commercially (Charles River). Once mice homozygous for these later two transgenes were identified, backcrossing these mice to the original stock and simple visual and PCR testing for *smn* and GFP were used to identify the animals of interest. Backcrossing of SMAΔ7;S100-eGFP mice (Jackson Labs stock number JR16573) has presently reached the 10th generation and no substantial alteration in the survival time of the homozygous null mice in the crossings has been noted.

Dietary supplementation of mutant SMAΔ7 mice

We tried in a few cases to extend the lifespan of the SMAΔ7 mice by supplementing their diet. For this purpose, animals were fed up to 10 times a day beginning at P2–8, with small quantities of an artificial diet formulated to simulate the protein content of rodent milk (one part of puppy milk replacement [1.7 g Esbilac in 10mls H_2O] to four parts human milk replacement [2 g Enfamil in 5mls H_2O] to a final concentration of 6.0 grams of protein per 100mls) (Barlow et al., 1974). This liquid diet was fed from a syringe attached to a small cannula pulled from polyethylene tubing by placing drops on the tongue and allowing the animals to swallow the drop. Such treatment led to weight gain and survival of animals. However, because the supplementation did not alleviate the spasticity of the animals or their failure to thrive, all these experiments were terminated before P21.

Tissue preparation and analysis

For electron microscopy (EM) of NMJs and morphometric analysis of nerves and muscle fibers, animals were perfused through the heart first with 0.1 M Sørensen's buffer (19 ml 0.2 M NaH_2PO_4, 81 ml 0.2 M Na_2HPO_4, pH 7.4) followed immediately by EM fix (2% paraformaldehyde and 3% glutaraldehyde in 0.1 M Sørensen's buffer). The sternomastoid, extensor digitorum longus (EDL) and soleus muscles were then exposed and fixed in situ for 30 minutes. Muscles were then dissected along with the associated nerve and fixed overnight in the same EM fix, then washed in three changes of Sorenson's buffer, 10 minutes each. The tissues were then stained en bloc with 2% potassium ferrocyanide and 2% osmium tetroxide for 2 hours, washed with distilled H_2O, stained with 2% uranyl acetate for 2 hours, washed with distilled H_2O, dehydrated in increasing concentrations of ethanol that was then changed to absolute acetone, and embedded in Epon 812 (Electron Microscopy Sciences, Hatfield, PA). Prior to embedding, muscle nerves were removed from associated muscle by cutting proximal to any branches at the site of muscle entry, embedded separately in Epon and oriented so that the distal ends of the nerves were sectioned first.

For counting muscle fibers, semi-thick cross-sections (~500 nm) were cut using glass knives and stained with 1% toluidine blue. Sections were made approximately midway between the muscle tendons so that no section counted contained tendon; therefore all the fibers in the muscle were counted. Digital images were captured of sections viewed under Normarski optics in a light microscope. For counting axons in the muscle nerve to soleus, cross-sections (65 nm) were made using a diamond knife and digital images captured with a transmission electron microscope (TEM; Tecnai, Hillsboro, OR). Montages of entire muscle and nerve cross-sections were made on a Macintosh computer (Apple Computer, Cupertino, CA) using Photoshop software (Adobe Systems, San Jose, CA). Measurements of muscle fiber size and counts, and axon counts and diameter as well as thickness of myelin were carried out using IPLab/iVision software (BioVision, Exton, PA) by manually tracing individual muscle fibers, axons and the myelin sheath.

For fluorescent labeling of muscle whole mounts, the animals were transcardially perfused with PBS, pH 7.4. The sternomastoid, EDL and soleus muscles were dissected and fixed in 4% phosphate-buffered paraformaldehyde, pH 7.4 for 20 minutes at room temperature and rinsed in three changes, 5 min. each, of PBS.

For muscle fiber type determination, the sternomastoid, EDL and soleus muscles were dissected from animals transcardially perfused with PBS, pH 7.4, and fresh-frozen in Tissue-Tech Optimal Cutting Temperature (OCT) compound (Ted Pella Inc., Redding, CA) with liquid nitrogen. The blocks of muscles were cut on a cryostat (Hacker Instruments, Winnsboro, SC) to produce 12-μm, serial sections at an angle perpendicular to the long axis of the muscle fibers.

Physiology

Soleus muscles were dissected, as described previously (Thompson, 1983b), with their innervation intact to the spinal cord to include the two ventral roots, L4 and L5, that contain motor axons to the muscle, and pinned to a Sylgard-coated dish and superfused with oxygenated Ringer's solution containing 2mM Ca^{++}. Muscle tension recordings were made at optimal muscle length by attaching the distal tendon to a sensitive strain gauge (A408; Cambridge Technology, Lexington, MA). Stimuli (1 ms duration) were applied to nerves via a suction electrode and a Grass S88 Stimulator; contractions were monitored using an oscilloscope. Direct muscle stimulation was accomplished by passing 100 V pulses of 1–2 ms duration applied between two platinum electrodes located on each side of the muscle belly. The number of motor units in each muscle preparation was determined by counting the threshold increments in tension generated as stimuli of gradually increasing strength were applied to the filaments teased from the ventral roots (Thompson, 1983b). If a filament contained more than 3 motor units, it was further teased and the resulting filaments analyzed to provide for more accurate counts.

Fluorescence immunohistochemistry

Muscles for whole-mount labeling of NMJs were prepared as described above and immunostained as described previously (Hayworth et al., 2006; Kang et al., 2007; Zuo et al., 2004). To label surface nicotinic acetylcholine receptor (AChR) at NMJs, fixed muscles were incubated with α-bungarotoxin (α-BTX, a snake toxin which binds specifically and with high affinity to AChR) conjugated to tetramethyl-rhodamine or Alexa647 (1:500; Invitrogen, Carlsbad, CA) prior to permeabilization. The presynaptic nerve terminals were labeled with a mixture of monoclonal antibodies (mAbs) to neurofilament and synaptic vesicles (2H3 and SV2, respectively; Developmental Studies Hybridoma Bank, University of Iowa, Iowa City, IA) and an anti-mouse antibody conjugated to FITC (Cappel, West Chester, PA). To assay for neurofilament accumulation in endplate area, a rabbit anti-

synaptophysin antibody (Invitrogen) and an anti-rabbit antibody conjugated to TRITC (Cappel) were used to label synaptic vesicles and with mAb 2H3. Synaptic basal lamina proteins, acetylcholine esterase (AChE) and laminin β2, were labeled with fasciculin2 (Sigma-Aldrich, St. Louis, MO) conjugated to cyanine5 (Cy5; Invitrogen), rabbit anti-laminin β2 antibody (Sasaki et al., 2002) and an anti-rabbit antibody conjugated to TRITC (Cappel), respectively. For counts of SCs, 4',6-Diamidino-2-phenylindole (DAPI; 0.5 μg/ml) was used as a stain for nuclei. For fiber typing, serial muscle cross-sections (see above) were stained with mouse monoclonal myosin heavy-chain (MHC) specific antibodies (Developmental Studies Hybridoma Bank) and anti-mouse antibodies conjugated to FITC (Cappel). The mAbs to MHC used were: A4.840 (type I; slow), A4.74 (type IIa), 10F5 (type IIb), 6H1 (type IIx), F1.652 (embryonic) and A4.1025 (pan MHC). Muscle fibers expressing a given MHC isoform were represented as a percentage of total number of myofibers in the muscle. Images were acquired using a Leica (Nussloch, Germany) DMR epifluorescence microscope equipped with a Hamamatsu cooled CCD camera controlled by a Macintosh computer with IPLab/iVision software.

Ultrastructural examination and 3-dimensional reconstruction of NMJs

EDL muscles from P14 mutant SMAΔ7 mouse and control littermates were processed for TEM as described above. Serial thin sections (65 nm) were made through a single synapse in each muscle using a diamond knife. Random sampling was also used to obtain images of other NMJs. EM images of synapses were captured with a digital camera and montages encompassing the synapse on one muscle fiber were prepared using Photoshop. A serial series of montaged TEM images from muscle serial sections were then used to create a 3-dimensional rendering of the NMJ and its cellular components using "Reconstruct" software (Fiala, 2005). Additionally, the following synaptic components were traced/segmented for quantitative comparison of mutant and control NMJs: secondary synaptic folds in postsynaptic muscle membrane, nerve/muscle contact, and synaptic vesicles. Vesicles were traced individually when possible, however, those in close proximity to others were traced as clusters when traces for individual vesicles would likely overlap.

Quantification of synaptic labeling

To differentially quantify the topology of postsynaptic AChR aggregates, we categorized each junction into one of the 4 types: simple plaque, perforated plaque, open or C-shaped and branched (Kummer et al., 2004). The same synapses were also scored for the junctional (or secondary) folds indicated by the presence of "stripes" of α-BTX label (Marques et al., 2000) and placed in one of the following 4 categories: no stripes (absent), short and disorganized stripes (disorganized), stripes over more than ~25% (partial) and ~75% (full) of the AChR aggregate. Statistical analysis of raw data and the generation of histograms were performed using Excel spreadsheet software (Microsoft, Redmond, WA). Numerical data are reported as mean ± SEM.

Results

Counts of motor units and axons suggest no significant motor neuron loss

The precise nature of the defects in the SMAΔ7 mice that phenocopy a severe form of human SMA remains unknown. If the disease were indeed produced by death of motor neurons, then physiological and histological analysis would be expected to reveal reductions in their number. Recognizing many of the difficulties of obtaining accurate motor neuron counts by histology of the spinal cord, we resorted to two alternative approaches: 1) counting axons in images from transmission electron micrographs of muscle nerves and 2) counting motor units as the increments in muscle twitch tension. We focused our efforts on

SMA end-stage animals (i.e. those at P12–14) since motor neuron death has been reported to be a late event in SMAΔ7 disease progression (Le et al., 2005).

First, examination of the electron microscopic images from P13 soleus nerves of 3 mutants and 3 control littermates (Fig. 1A,A') showed no difference in the number of axons, either myelinated or unmyelinated (Fig. 1B). In addition, there was no difference in the degree of myelination of axons in the motor nerves as assessed by g-ratio measurements (Fig. 1C). Our detailed analysis of axon number and their state of myelination as a readout of their integrity in control and mutant nerves confirms the initial qualitative assessment of SMAΔ7 mutant nerves by Sumner and colleagues (Kong et al., 2009), and argues against the idea that motor neuron axons are dying back from their target muscle fibers (McGovern et al., 2008). While the axon count suggests there is not an obvious loss of motor neurons, it provides no information on the functional health of these motor neurons. Therefore, to be certain that the number of healthy motor neurons was indeed unaltered, we estimated the number of motor units in soleus muscles from a set of mutants and their littermate controls at P12–14 by counting increments in the twitch tension from stimulating filaments teased from the ventral roots. Since this method assays tension development from nerve stimulation, it determines whether motor neurons make functional connections with muscle fibers. The number of units found in control muscles was 16, 15,13 and 15 (4 muscles from 4 animals); those in mutant muscles were 14, 15, 13, 14 (4 muscles from 4 animals) (Fig. 2A). Thus, there appears to be no significant loss of motor neurons in soleus muscles even at the end-stage of disease progression in SMAΔ7 mice.

The apparent lack of motor neuron death in mice is not consistent with reports for the human disease. One possible explanation of the inconsistency is that the mice die before motor neuron deficits become evident. Indeed, the mutant SMAΔ7 mice may cease to feed from their mother and this may contribute to their death. We found that these mutant mice could be maintained for a longer period by hand-feeding an artificial diet. We carried out 3 supplemental feeding experiments that were terminated at P17, P20 and P21. The supplemented animals outlived other mutant animals and responded with a modest but significant increase in body weight. At P13 supplemented pups weighed 4.2 ± 0.4 g compared to 3.0 ± 0.1 g for non-supplemented littermates ($n \geq 6$, $p < 0.01$); at P19 supplemented pups had continued to gain some weight, reaching 4.8 ± 0.2 g ($n=3$). The number of motor units counted in these mutant muscles was 13, 16 and 16, comparable to those counted in soleus muscles of mutant or controls at P12–14 (Fig 2A). Counts of axons and motor units, together, provide the most definitive functional evidence to date that disease pathology in SMAΔ7 mutant mice, at least in the soleus muscle, is not due to death of motor neurons or dying back of their axons from their muscular targets. These findings are also in agreement with a report from Monani and colleagues where motor neuron death is a relatively late event in SMAΔ7 disease progression (Le et al., 2005) and where motor deficits precede motor neuron death in a new SMA mouse model (Park et al., 2010b). Therefore, even at an age beyond its normal lifespan, there appeared to be no apparent deterioration in the number of functional motor units in the soleus muscle of mutant SMAΔ7 mice.

Mutant soleus muscle contractions are consistent with reduction in muscle mass without gross defects in neuromuscular transmission

As our histological and physiological assays suggested no significant loss of motor neurons, we asked whether the motor deficits of SMAΔ7 mice (Butchbach et al., 2007) could be attributed to failure of synaptic transmission at the mutant neuromuscular junction. Soleus muscles, together with their nerves, were dissected from the hindlimbs of SMAΔ7 mutant mice and their unaffected littermates, and the tension generated in response to suprathreshold stimulation of the muscle nerve measured. Consistent with the smaller size of

the mice themselves (Le et al., 2005), mutant soleus muscles were noticeably smaller than their control counterparts at P13 (see below; Fig. 3A). The contractions of the muscles were measured in response to stimulus frequencies giving fused and unfused tetani (Fig. 2B). While mutant muscles always gave half or less the tension of control muscles, they responded faithfully to each nerve stimulus with a contraction. This high fidelity of neuromuscular transmission was maintained in soleus muscles isolated from mutant SMAΔ7 animals maintained past their normal lifespan by means of supplemental diet (data not shown). In addition, the mutant muscles maintained tension as competently as littermate controls even when subjected to stimulation for 7.5 seconds at 100 Hz to produce a fused tetanus (Fig. 2C). The ability of mutant muscles to respond to each nerve stimulus and hold tension suggests that neuromuscular function remains suprathreshold. Lastly, direct stimulation of the muscle yielded the same twitch tension as did nerve stimulation (data not shown), suggesting there is not an extensive population of denervated fibers in the mutant muscle. Therefore, the weakness of SMNΔ7 soleus muscles is unlikely to result from loss of innervation to individual muscle fibers in soleus muscles. It appears that cholinergic transmission at the NMJs remains intact and our results are in good agreement with a recent report of effective transmission at SMAΔ7 mutant NMJs (Ling et al., 2010). Thus, the muscle weakness in mutant SMAΔ7 mice may be a consequence of the smaller size of the muscles or some kind of inability to execute functional motor patterns in the spinal cord.

Impaired postnatal growth of SMAΔ7 mutant muscles

The reduction in muscle mass observed in SMAΔ7 mutant mice could result from smaller and/or fewer individual muscle fibers. Gross examination of muscle cross-sections used for muscle fiber typing suggested that the mutant muscle fibers are significantly smaller (Fig. 3A). To explore this issue more thoroughly, we examined muscles at P13. In attempt to prevent unintended alterations of muscle fiber cross-sectional area during processing of the tissue, we fixed muscles in situ at resting muscle length. After post-fixation and embedding in epon, semi-thick (500μm), plastic sections were examined in the light microscope. Consistent with previous reports (Kong et al., 2009; Le et al., 2005), the average cross-sectional area of P13 mutant soleus muscles is significantly reduced compared to that of control littermates (168 ± 2 vs. 764 ± 8 μm^2; *** P<0.001, Students T-test) (Fig. 3B). More importantly and not previously noted, the distribution of individual fiber areas (Fig. 3C,D) shows that mutant fibers are uniformly decreased in diameter. This suggests that there is not a subpopulation of motor neurons dying and leaving denervated fibers. Rather, it appears that whatever is altering the size of the muscles alters every fiber in the muscle. We also observed the same uniform reduction in fiber size in two additional muscles examined, the sternomastoid (mean: 311 ± 2 vs. 746 ± 4 μm^2; *** P<0.001; Fig. 4) and EDL (mean: 169 ± 2 vs. 583 ± 6 μm^2; P<0.001; and data not shown). Thus, the reduction of SMN expression appears to produce a reduction of muscle fiber size in both a slow and fast twitch muscle in the leg and a proximal and anterior fast muscle. Given the small size of the animals, it is likely this reduction occurs in many, if not all, muscles throughout the animal.

To determine whether this reduction in muscle fiber size is due to impaired muscle fiber growth or to atrophy, we compared muscles at P13 with those present at an earlier time, P5. P5 control soleus muscle fibers are significantly larger than those in the P5 mutants, although the difference in size (Fig. 3B; 171 ± 2 vs. 220 ± 2 μm^2; *** P<0.001) is much less than at P13. Again, the distribution in sizes shows that the size reduction at P5 is not in a subpopulation of fibers (Fig. 3C,D). While the control muscle fibers undergo tremendous growth in size the next 8 days (from 220 ± 2 to 764 ± 8 μm^2), the mutant muscles do not grow (from 168 ± 2 to 171 ± 2 μm^2). A similar result is obtained for the sternomastoid muscle fibers (Fig. 4B,C): a uniform reduction in size is evident at P5 (206 ± 2 vs. 262 ± 2 μm^2; *** P<0.001) and their growth during the next 8 days is significantly impaired

compared to controls (from 206 ± 2 to 311 ± 2 μm^2 vs. from 262 ± 2 to 746 ± 4 μm^2). Thus our findings are consistent with those of Sumner and colleagues (Kong et al., 2009) and argue that muscles of SMAΔ7 mutant mice do not undergo atrophy, but rather fail to grow in size during their early postnatal development.

It is possible that this lack of postnatal muscle development is strictly a consequence of the SMAΔ7 mutant mice to thrive. However, in analyzing a soleus muscle from a hand fed P17 mutant mouse (Fig. 3A), we found that the average fiber size (170 ± 2 μm^2) and distribution of fiber sizes are unaltered when compared to those from non-supplemented P13 mutant soleus muscles (Fig. 3D), further suggesting that mutant muscle fibers are not undergoing atrophy. In contrast, SMAΔ7 mutant mice that are supplemented with an artificial diet continued to grow and were significantly bigger, at P17, than non-supplemented P13 mutants (4.45 g ± 0.31 vs. 3.09 g ± 0.13; $n \geq 4$; $p < 0.001$). Therefore, the retarded growth of mutant muscle and its fibers can be decoupled from the animals' body weight and inability to grow. Moreover, electron microscopic examination of individual muscle fibers from both control and mutant P13 soleus muscles failed to reveal ultrastructural changes associated with atrophy (Lu et al., 1997) such as disorganization of sarcomeric structures and loose folds of basal lamina in and around mutant muscle fibers (Fig. S1).

Mutant soleus muscles, but not sternomastoid or EDL muscles, displayed an additional difference from the same muscles in normal siblings. At P13, mutant soleus muscles had 15% fewer fibers than those of control littermates (532 ± 14 vs. 623 ± 26 or 86 ± 3 % of control; n=3, * $p < 0.05$; Fig. 3E). There also appeared to be fewer fibers in mutant soleus muscles at P5 (490 ± 7 vs. 552 ± 64 or 90 ± 12 % of control; n=3, $p > 0.469$; Fig. 3E), although the difference did not reach statistical significance. The deficit in fiber counts persisted in soleus muscles of 2 animals fed with an artificial diet (387 and 497, at P17 and P21 respectively, compared to 628 and 618 of age-matched littermates). Although the small sample size limits statistical analysis, there appeared to be a small reduction in the number of mutant soleus fibers after P13. Thus, the mutant muscle fibers may become more susceptible to damage and degeneration over time. A similar reduction in the number of fibers was found in a mutant EDL muscle at P17 (1037 compared to 1353 for a control littermate). Any loss of fibers in the hindlimb muscles did not appear to be compensated for by regeneration as the proportion of fibers with centrally located nuclei, a marker for regenerated fibers, was comparable in mutant muscles and controls (data not shown). Interestingly, skeletal muscle progenitor cells, a subset of muscle satellite cells that are essential for muscle growth and repair, have been reported to exit early from the cell cycle and undergo premature differentiation in SMA muscles (Bennett, M.H., Cerletti, M.,Wagner, A., Wagers, A., and Rubin, L.L. 2009 American Society for Cell Biology meeting abstract #428). Therefore, the deficit in muscle fiber number in soleus seen at the terminal stage of disease may result from a reduced capacity for muscle growth and repair of damaged fibers.

Pattern of myosin heavy chain expression reveals lack of myofiber maturation in SMAΔ7 mutant mice

Defects in postnatal generation and/or growth of muscle fibers suggested that SMAΔ7 mutant muscle fibers might also be less mature than those in the control muscles. Sumner and colleagues reported alteration of mRNA levels of individual MHC isoforms in SMAΔ7 mutant hind leg muscles that is consistent with lack of postnatal maturation (Kong et al., 2009) – increased perinatal isoform vs decreased adult isoforms. To directly test whether these defects represent global changes across muscles at the protein level and whether individual muscle fibers continue to differentiate, cross-sections of P12 control and mutant SMAΔ7 sternomastoid and soleus muscles were labeled with isoform-specific anti-MHC monoclonal antibodies (Condon et al., 1990a, b). Fibers labeling for slow myosin were

present in a scattered pattern in the deep portion of sternomastoid muscles of both control and mutant animals (Fig. 5B,B'). In soleus muscles, fibers labeling for slow myosin were more prevalent and were scattered throughout both control and mutant muscles. Thus, slow fibers appear in the expected locations in these muscles and there is no evidence for clustering of these slow fibers into contiguous groups as might be expected if the fibers had undergone rounds of denervation and reinnervation by sprouts ("fiber type grouping"). Interestingly, however, we found a muscle-specific reduction in the abundance of muscle fibers expressing fast myosin in mutant muscles when these were compared to their controls (type IIx and IIb in sternomastoid, and type IIa in soleus; Fig. 5A,A',D). In addition, there was a small but significant increase in the proportion of muscle fibers that expressed the embryonic isoform of myosin heavy chain in sternomastoid muscles of the SMAΔ7 animals (Fig. 5C). Consistent with the normal slower development of soleus compared with more anterior muscles (Condon et al., 1990a), virtually all the fibers in both control and mutant soleus expressed embryonic MHC. These findings are also consistent with persistent expression of embryonic MHC isoform in muscles from a different SMA model (Biondi et al., 2008), and in human SMA patients (Martinez-Hernandez et al., 2009; Stevens et al., 2008), but provide additional information that the regional differentiation of fiber types within muscles is maintained. Taken together, these findings suggest that fibers in mutant muscles, in addition to their smaller sizes, are generally less mature than those in controls.

Muscle-specific impairment of neuromuscular synaptic morphology in SMAΔ7 mutant mice

To determine whether there were alterations in the morphology of NMJs in SMAΔ7 mice, we fluorescently labeled motor axons, presynaptic nerve terminals, and postsynaptic muscle membranes with antibodies to neurofilament and to synaptophysin, and with fluorochrome conjugated α-BTX, respectively (Fig. 6A). Pre- and postsynaptic labels resemble each other in shape and occur in good register. We failed to detect any obvious signs of denervation or terminal sprouts originating from intact NMJs in all 3 muscles examined between P10 and 14 (data not shown; also see (Kong et al., 2009; Ling et al., 2010)). However, a closer examination of mutant NMJs and their cellular components revealed muscle-specific defects in synaptic maturation. First, approximately 40% of the endplates in SMAΔ7 mutant sternomastoid muscle were apparently polyneuronally innervated based on the entry into the synaptic site of two or more preterminal axons. In many cases these preterminal axons could be followed for a distance ranging from 37 to 95 microns (70 ± 4 μm; n=13 polyneuronally innervated endplates) along the pathway leading to the synaptic site, suggesting they are branches of different rather than the same motor neurons. In contrast, no polyneuronally innervated junctions were found among the control sternomastoid NMJs examined (Fig 6B). No difference in polyneuronal innervation of control and mutant soleus muscles was found. Here, however, both the mutant and control muscles had a significant number of endplates that appeared to be multiply innervated, and any difference in the extent of polyneuronal innervation, if present, would be less obvious. We interpret these findings as showing a delay in the loss of polyneuronal innervation in an anterior muscle; this delay however is not obvious in more posterior muscles where normally polyneuronal innervation is lost later in development.

Consistent with previous characterization of NMJs in SMA mouse models (Cifuentes-Diaz et al., 2002; Kariya et al., 2008; Kong et al., 2009; Murray et al., 2008), we found abnormal accumulations of neurofilaments at mutant synapses. However, as was the case with delay in elimination of polyneuronal innervation, sternomastoid muscles were more severely affected than soleus muscles (Fig. 6C): 97 ± 1% and 76 ± 6% (n=3; $p<0.05$) of NMJs in sternomastoid and soleus, respectively, displayed neurofilament accumulation. Interestingly, the morphology of the neurofilament accumulations also differed between the two muscles

(Fig. 6A). Virtually, all of the neurofilament accumulations in NMJs of sternomastoid appeared “bulbous” and extended to the very tips of the nerve terminals (asterisk in Fig. 6A; SMA, 94.4 ± 0.7% vs. Control, 7.38 ± 0.6%; $p<0.001$). In contrast, more than half of soleus NMJs with neurofilament accumulation had a “frayed” or “webbed” appearance of the presynaptic axons (§ in Fig. 6A; SMA, 54.14 ± 6.67% vs. Control, 32.3 ± 4.95%; $p<0.001$). Explanations for the disorganization in neurofilaments are presently lacking.

Postsynaptic AChR aggregates initially appear as simple plaques and become successively more complex as “perforated” plaques, “C”-shaped, branched configurations, and eventually mature “pretzels” (Kummer et al., 2004). This progressive differentiation is severely stunted in NMJs in mutant sternomastoid muscles (Fig. 7A) in agreement with reports of postsynaptic morphology at mutant NMJs (Kariya et al., 2008; Kong et al., 2009). In P12 control sternomastoid, virtually all AChR aggregates have evolved past the plaque stage and have obtained open-configurations (C-shaped or branched). In the sternomastoid of mutant siblings, more than 40% of receptor aggregates are still plaque-shaped and only about 20% have reached the open configurations, while the remaining 40% have undergone partial transformation and are perforated. Interestingly, the defects in AChR maturation are less evident in mutant soleus and EDL muscles (Fig. 7B); however, even control junctions of these muscles are immature at this stage of postnatal development, consistent with the known anteriorposterior gradient in development of neuromuscular synapses. Mutant NMJs are also defective in forming secondary junctional folds (Fig. 7A,C; also see below), another indicator of postsynaptic differentiation. Junctional folds, which appear as stripes of BTX labeling in NMJs viewed en face in the confocal microscope (Marques et al., 2000) are present in parts or all of the postsynaptic area in more than 70% of NMJs in P12 control sternomastoid muscles. In contrast, a large majority of NMJs in sternomastoid muscles of mutant littermates show patchy, short and/or disoriented stripes of AChR aggregates (Fig. 7B). Differences between the pattern of striping in control and mutant junctions of soleus and EDL muscles are far less obvious (Fig. 7B); even control junctions appear relatively immature in this feature. Thus, just as the case for polyneuronal innervation presented above, the differences in control and mutant junctions are present in those muscles more advanced in development and less obvious in those that are immature.

The vertebrate NMJ is a tripartite synapse. In addition to the presynaptic motor nerve terminal and the postsynaptic muscle membrane, terminal Schwann cells (tSCs) at the NMJs are critical for structural integrity and growth of the synaptic contact (Reddy et al., 2003). To examine the number and distribution of non-myelinating tSCs at the junction we introduced into the SMAΔ7 mutant mice a transgene coding for expression of soluble GFP by interbreeding with the previously described Kosmos transgenic line (Zuo et al., 2004). The number of tSCs is significantly reduced in mutant mice (Fig. 8A–C). This deficit was evident in both sternomastoid (2.1 ± 0.1 vs. 4.9 ± 0.1 per mutant and control NMJ, respectively; $n\geq149$ junctions from 2 control and SMA animals, *** $p<0.001$) and soleus muscles (2.4 ± 0.08 vs. 3.6 ± 0.1 per mutant and control NMJ, respectively; $n\geq143$ junctions from 2 control and SMA animals, *** $p<0.001$). This reduction in number is correlated with reduced endplate area (Fig. 8D) which, in turn, is likely due to the smaller muscle fibers (Love and Thompson, 1998). In addition, we found the coverage of postsynaptic AChR aggregates by the terminal SCs to be incomplete at some mutant NMJs in contrast to control synapses (example in Fig. 8B; see also Fig. 10C’). As the cell bodies of SCs normally arrive at the NMJ after the synapse has been formed (Love and Thompson, 1998), the reduced number and incomplete coverage suggests abnormal or delayed development of SMAΔ7 NMJs. Given that tSCs in turn play an important role in the growth and physiology of developing NMJs (Reddy et al., 2003), SMA junctions are deficient here as well.

As a recent report has provided evidence of wide-spread splicing defects in SMAΔ7 mice and suggested that long transcripts – many of which yield extracellular matrix proteins – are more susceptible to aberrant splicing in mutant mice (Zhang et al., 2008), we tested whether there were alterations in the localization of components of the synaptic basal lamina. We examined the localization of the enzyme acetylcholine esterase and of laminin β2 (s-laminin), which has recently been demonstrated to organize active zones of motor axon terminals (Nishimune et al., 2004). These were seen to co-localize with the postsynaptic AChR at both control and mutant NMJs (Fig. S2); thus there is no obvious deficiency in synaptic distribution of these molecules.

Ultrastructural examination of mutant SMAΔ7 NMJs

In an attempt to better understand the structural changes that occur at the synapses in the mutant muscles, we examined several control and mutant NMJs between P10 and 14 in the electron microscope. A sampling of NMJs encountered in random sections in these muscles suggested that there were several alterations (Fig. 9A,A'): postsynaptically, there were fewer and shallower secondary junctional folds; presynaptically, nerve terminals had fewer and more scattered synaptic vesicles.

To extend and quantify these preliminary observations on the ultrastructural changes in SMA muscles, we prepared three-dimensional (3D) renderings of serial electron micrographs of NMJs from a control and a mutant P14 SMAΔ7 EDL muscle. A set of approximately 100 serial, ultrathin (65 nm) sections, representing coverage of approximately 6.5 μm along the long axis of the muscle fiber, were collected. Digital images were prepared of the junction in each section and these sections aligned in software. Each structure of interest - the nerve terminal, the SCs, synaptic vesicles, and the junctional folds in the muscle membrane - were segmented in software. Three-D projections of these images were prepared and segmented objects quantified. Presynaptically, the 3D rendering of control and mutant nerve terminal viewed from above (Fig. 9B,B') showed that the mutant nerve terminal is smaller and less branched. In fact, in contrast to the control junction, there were no interruptions in the cytoplasm of this mutant nerve terminal where it was in close contact with the muscle fiber membrane. These features are consistent with the simplified morphology of nerve and AChR in the mutant junctions seen in the light microscopy (Fig. 7A,B). Additional defects were found upon closer examination. There was a reduction in the number of synaptic vesicles in the mutant nerve terminal: vesicles in the mutant nerve terminal occupied a volume of 5.43 μm^3 compared to 12.01 μm^3 in controls. Even after correcting for the smaller size of their nerve terminals, the mutant had roughly 1/3 fewer vesicles (21.7% of the volume in the mutant terminal vs. 33.7% in the control), consistent with recent reports of reduced vesicle pool and quantal size of SMAΔ7 mutant motor nerve terminals (Kong et al., 2009; Ling et al., 2010; Ruiz et al., 2010). In addition, despite occupying a smaller portion of the nerve terminal the vesicles were more dispersed in the mutant: there were more vesicle clusters (8311 vs. 4437) and these clusters were smaller in size. The most profound and obvious change was found postsynaptically. Secondary junctional folds were reduced in the muscle fiber membrane in the SMAΔ7 mice (Fig. 9C,C'); the volume of the secondary folds was about 14 fold greater in controls after normalizing for the area of synaptic contact (0.081 vs. 0.006 $\mu m^3/\mu m^2$). This reduction is consistent with the inferences from our light microscopic observations (Fig. 7A,C) and, since such folds are added gradually during early postnatal development (Marques et al., 2000), consistent with a developmental delay in the SMA muscles. While cellular and molecular mechanism(s) responsible for formation of junctional folds are unclear, the deficit in the SMA muscles may be related to a marked reduction in the number and frequency of vesicles associated with postsynaptic membrane (Fig. 9A,A' inset). These vesicles appear to have fused with the plasma membrane in some instances and have flask-shape profiles

reminiscent of caveolae (Woodman et al., 2004). We find less than ½ the number of these postsynaptic vesicles per unit length of synaptic contact at the mutant synapse compared to the control (1.6 per μm vs. 3.4 per μm, respectively) while their overall density did not differ between control and SMAΔ7 mutant samples (each with 2.4 per μm). Lastly, likewise in agreement with results from fluorescence microscopy, SC-coverage of the mutant nerve terminal appears incomplete (Fig. 9C'; double arrowhead).

Discussion

Despite knowledge of the genetic basis of SMA and generation of mouse models, the cell type(s) and the cellular process(es) responsible for its pathology remain elusive. This is an important issue in designing potential therapeutic interventions. One key question is if and why SMA is a disease specifically of motor neurons, given the ubiquitous requirement for SMN protein (Cifuentes-Diaz et al., 2001; Frugier et al., 2000; Schrank et al., 1997; Vitte et al., 2004). The emphasis on motor neurons comes from the profound muscle weakness in human patients and the evidence of motor neuron loss from postmortem examination of both humans (Crawford and Pardo, 1996) and of SMA mouse models (Hsieh-Li et al., 2000; Jablonka et al., 2000; Le et al., 2005). Attempts at tissue-specific alteration in SMN expression have suggested motor neuron involvement (Azzouz et al., 2004; Foust et al., 2010; Gavrilina et al., 2008; Park et al., 2010b), but failed to demonstrate that SMA results from SMN reduction only in motor neurons. Moreover, reports of defects in other cell/tissue types in SMA models (Heier et al., 2010; Liu et al., 2010; Shababi et al., 2010; Wishart et al., 2010) illustrate that SMA is a complex disease; it cannot be explained by a simple deterioration of neuromuscular connections. Even if motor neuron expression is key, studies have now shown alterations in the synaptic inputs to the motor neurons themselves play a significant role in SMA pathogenesis (Ling et al., 2010; Mentis et al., 2011; Park et al., 2010b)

A key finding of our study of SMNΔ7 mice is a profound delay in postnatal neuromuscular development in a set of muscles without evidence of motor neuron loss or overt failure of neuromuscular transmission. The loss of force generated by these mutant muscles is explained, not by deficiencies in their innervation, but by the small size of their muscle fibers. The lack of a deficiency in neuromuscular transmission is consistent with other observations in SMAΔ7 mutants (Kong et al., 2009; Ling et al., 2010; Ruiz et al., 2010). It might be argued that a different set of muscles than the soleus we chose for our physiological examinations are those most affected by the disease. Indeed, there is now strong evidence that a set of motor neurons in the medial motor column do die in this mouse model and death here is much more prominent than in the lateral motor column (Mentis et al., 2011). A death of motor neurons to some muscles is also supported by other studies (Kariya et al., 2008; Kong et al., 2009; Murray et al., 2008). However, the muscles we studied are clearly altered by the disease. They show a similar reduction in fiber size and this reduction is uniform across all the fibers in these muscles. This finding is inconsistent with a progressive disease affecting motor neuron after motor neuron in these muscles; such a mechanism would be expected to produce alterations within individual motor units in the muscles and we observed no evidence of such alterations. Rather, it appears that the disease is uniformly altering all the motor neurons to the 3 muscles we studied or alternatively all the fibers in these muscles. A possible explanation for some of the discrepancies among the different mouse models in motor neuron death and synaptic failure may simply be how rapidly and generally the disease state progresses and how long the mice live following onset of symptoms. For example, neurofilament accumulation is more pronounced in SMAΔ7 mutants than in genetically identical mice that lack the SMNΔ7 transgene and that succumb to the disease ~10 days earlier (Murray et al., 2008). Therefore, if the disease is mild, progression of the disease might manifest as motor neuron death and synaptic failure

(Kariya et al., 2008; Park et al., 2010b) whereas if the disease progresses rapidly, the mice might die from other causes before motor neuron death itself. Findings in our own study suggest that supplementation of the diet of the SMAΔ7 mice so as to extend their life span results in an exaggeration of some of the defects but we still found no evidence for motor neuron death. Lastly, given the well-known trophic interdependence of motor neurons and their muscle fiber targets and the profound deficits in muscle fiber growth and maturation seen in the SMAΔ7 mice, it would not be surprising if motor neuron death in the cases where it is observed is a consequence of this interdependency (Habgood et al., 1984).

A consistent finding of our study is severe defects in the postnatal maturation of muscle and neuromuscular synapses. Postsynaptically, consistent with a pair of recent reports (Biondi et al., 2008; Kong et al., 2009), the muscle fibers are slowed in their loss of embryonic myosin and fail to gain the levels of fast myosin that are present in controls, even though the muscle-specific distribution of fiber types is retained. The muscle fibers are small because they fail to grow in size. The postjunctional folds fail to develop/mature and the AChR plaques remain immature in morphology and, from the observations of others, retain the fetal form of the AChR (Kong et al., 2009). Presynaptically, the motor nerve terminal fails to produce the normal number and distribution of synaptic vesicles. Many of the fibers retain polyneuronal innervation far longer than expected. Others have reported altered kinetics of endplate current and reduction in quantal content (Kong et al., 2009; Ling et al., 2010; Ruiz et al., 2010) consistent with immature NMJs. Additionally, there are fewer tSCs at mutant NMJs and their coverage of the nerve terminals is less complete. All of these descriptors are characteristic of younger stages of neuromuscular development, suggesting SMA slows this development. It is unclear why so many different aspects of neuromuscular development should be slowed, but neuromuscular activity is well known to be a critical factor here. For example, synaptogenetic protein agrin alone is sufficient to drive many aspects of neuromuscular differentiation, including aggregation of AChR and selective gene transcription from postsynaptic nuclei (Cohen et al., 1997). However, more complete differentiation requires activity of postsynaptic muscle fiber as well: stimulation of activity in an otherwise denervated muscle can induce the γ to ε subunit (fetal to adult isoform) switch in AChR receptor composition (Brenner et al., 1987; see also Rimer et al., 1997) and maintain the metabolic stability of AChR in the postsynaptic membrane (Andreose et al., 1993). Similarly, neuromuscular activity profoundly affects the postnatal loss of polyneuronal innervation (Thompson, 1983a; Thompson et al., 1979), and postjunctional fold formation is severely stunted following denervation (Marques et al., 2000) and in animals that lack cholinergic transmission (Misgeld et al., 2002). A study using cultured myotubes suggests that electrical activity may also influence the organization of sarcomeres (Dutton et al., 1993); this is also shown by in vivo studies (see for example Bezakova and Lomo, 2001). One factor that could alter the activity of SMA motor neurons is the decrease in excitatory synaptic inputs the motor neurons themselves receive (Ling et al., 2010; Mentis et al., 2011; Park et al., 2010b), resulting in formation of silent or less active NMJs that are fully competent for faithful cholinergic transmission (Ruggiu et al., 2009). In this regard it is interesting to note that increased use of the neuromuscular system in some mouse models of SMA leads to amelioration of some of the symptoms (Biondi et al., 2008).

While it is tempting to attribute many of the developmental delays we see in SMA-afflicted mice to altered neuromuscular activity, it is clear some aspects of the development of the NMJ are activity independent. For example, aspects of the nerve contact area, including the partial maturation of receptors from plaque-like to a circular configuration can occur in the absence of production and release of ACh (Misgeld et al., 2002) or in cultured muscle fibers in the complete absence of neurons (Kummer et al., 2004). Similarly, some evidence suggests that the development of postjunctional folds depends only on the deposition of agrin (Cohen et al., 1997). There is also genetic evidence that molecules within muscle

fibers or the extracellular matrix modify this folding (Adams et al., 2000; Noakes et al., 1995). Additionally, as astrocytes produce molecules that potentiate synaptogenesis (Christopherson et al., 2005), the overall reduction in synapse density (Park et al., 2010b) and increased motor neuron-microglia interactions (Ling et al., 2010) suggest possible glial involvement in SMA pathogenesis. Our results of deficits in tSC number and their coverage of NMJs are consistent with this hypothesis. Together, these observations emphasize the complexity of the etiology of this disease and suggest it cannot be simply explained by decreased activity of motor neurons either.

Interestingly, in mouse tissues it appears that SMN expression is highest during embryonic and early postnatal stages and declines rapidly thereafter (Gabanella et al., 2005). In addition, the maximum efficacy of a virus-mediated replacement therapy in SMA mice was achieved with early postnatal initiation (P2) and declines rapidly thereafter (Foust et al., 2010). This raises the possibility that sensitivity to SMN reduction is highest in younger animals and results in severe forms of SMA, such as that present in the SMNΔ7 mouse used in this study, and this early reduction leads to developmental delays (Hausmanowa-Petrusewicz and Vrbova, 2005) such as reported here. However, a reduction in SMN that occurs later in development or is less severe might produce an entirely different disease. This also suggests the time requirements for effective therapeutic interventions might be quite different among the different forms of SMA.

Highlights

- Normal complement of motor units present in the SMAΔ7 mouse model.
- SMAΔ7 mutant muscles are weaker due to a uniform reduction in fiber diameter.
- No exaggeration of symptoms in mutant mice maintained past life expectancy.
- Overall neuromuscular development is stunted in SMAΔ7 mutant mice.

Supplementary Material

Refer to Web version on PubMed Central for supplementary material.

Acknowledgments

We thank the SMA Foundation for providing the SMAΔ7 mice and for funding for this work, Mary Ann Mann for her help in genotyping mice, Dr. Takako Sasaki (Friedrich-Alexander University, Erlangen, Germany) for her generous gift of anti-laminin β2 antibody, and Dr. Glen Otto for calling our attention to the diet supplementation for rodents. This work was also supported by a grant from the NIH (NS20480).

References

Adams ME, Kramarcy N, Krall SP, Rossi SG, Rotundo RL, Sealock R, Froehner SC. Absence of alpha-syntrophin leads to structurally aberrant neuromuscular synapses deficient in utrophin. The Journal of cell biology. 2000; 150:1385–1398. [PubMed: 10995443]

Andreose JS, Xu R, Lomo T, Salpeter MM, Fumagalli G. Degradation of two AChR populations at rat neuromuscular junctions: regulation in vivo by electrical stimulation. J Neurosci. 1993; 13:3433–3438. [PubMed: 8340816]

Azzouz M, Le T, Ralph GS, Walmsley L, Monani UR, Lee DC, Wilkes F, Mitrophanous KA, Kingsman SM, Burghes AH, Mazarakis ND. Lentivector-mediated SMN replacement in a mouse model of spinal muscular atrophy. The Journal of clinical investigation. 2004; 114:1726–1731. [PubMed: 15599397]

Barlow B, Santulli TV, Heird WC, Pitt J, Blanc WA, Schullinger JN. An experimental study of acute neonatal enterocolitis--the importance of breast milk. J Pediatr Surg. 1974; 9:587–595. [PubMed: 4138917]

Bezakova G, Lomo T. Muscle activity and muscle agrin regulate the organization of cytoskeletal proteins and attached acetylcholine receptor (AchR) aggregates in skeletal muscle fibers. The Journal of cell biology. 2001; 153:1453–1463. [PubMed: 11425875]

Biondi O, Grondard C, Lecolle S, Deforges S, Pariset C, Lopes P, Cifuentes-Diaz C, Li H, della Gaspera B, Chanoine C, Charbonnier F. Exercise-induced activation of NMDA receptor promotes motor unit development and survival in a type 2 spinal muscular atrophy model mouse. J Neurosci. 2008; 28:953–962. [PubMed: 18216203]

Brenner HR, Lomo T, Williamson R. Control of end-plate channel properties by neurotrophic effects and by muscle activity in rat. J Physiol. 1987; 388:367–381. [PubMed: 2443692]

Burghes AH, Beattie CE. Spinal muscular atrophy: why do low levels of survival motor neuron protein make motor neurons sick? Nat Rev Neurosci. 2009

Butchbach ME, Edwards JD, Burghes AH. Abnormal motor phenotype in the SMNDelta7 mouse model of spinal muscular atrophy. Neurobiology of disease. 2007; 27:207–219. [PubMed: 17561409]

Christopherson KS, Ullian EM, Stokes CC, Mullowney CE, Hell JW, Agah A, Lawler J, Mosher DF, Bornstein P, Barres BA. Thrombospondins are astrocyte-secreted proteins that promote CNS synaptogenesis. Cell. 2005; 120:421–433. [PubMed: 15707899]

Cifuentes-Diaz C, Frugier T, Tiziano FD, Lacene E, Roblot N, Joshi V, Moreau MH, Melki J. Deletion of murine SMN exon 7 directed to skeletal muscle leads to severe muscular dystrophy. The Journal of cell biology. 2001; 152:1107–1114. [PubMed: 11238465]

Cifuentes-Diaz C, Nicole S, Velasco ME, Borra-Cebrian C, Panozzo C, Frugier T, Millet G, Roblot N, Joshi V, Melki J. Neurofilament accumulation at the motor endplate and lack of axonal sprouting in a spinal muscular atrophy mouse model. Human molecular genetics. 2002; 11:1439–1447. [PubMed: 12023986]

Cohen I, Rimer M, Lomo T, McMahan UJ. Agrin-induced postsynaptic-like apparatus in skeletal muscle fibers in vivo. Mol Cell Neurosci. 1997; 9:237–253. [PubMed: 9268503]

Condon K, Silberstein L, Blau HM, Thompson WJ. Development of muscle fiber types in the prenatal rat hindlimb. Developmental biology. 1990a; 138:256–274. [PubMed: 2108065]

Condon K, Silberstein L, Blau HM, Thompson WJ. Differentiation of fiber types in aneural musculature of the prenatal rat hindlimb. Developmental biology. 1990b; 138:275–295. [PubMed: 2318339]

Crawford TO, Pardo CA. The neurobiology of childhood spinal muscular atrophy. Neurobiology of disease. 1996; 3:97–110. [PubMed: 9173917]

Dutton EK, Simon AM, Burden SJ. Electrical activity-dependent regulation of the acetylcholine receptor delta-subunit gene, MyoD, and myogenin in primary myotubes. Proceedings of the National Academy of Sciences of the United States of America. 1993; 90:2040–2044. [PubMed: 8383334]

Fiala JC. Reconstruct: a free editor for serial section microscopy. J Microsc. 2005; 218:52–61. [PubMed: 15817063]

Foust KD, Wang X, McGovern VL, Braun L, Bevan AK, Haidet AM, Le TT, Morales PR, Rich MM, Burghes AH, Kaspar BK. Rescue of the spinal muscular atrophy phenotype in a mouse model by early postnatal delivery of SMN. Nat Biotechnol. 2010; 28:271–274. [PubMed: 20190738]

Frugier T, Tiziano FD, Cifuentes-Diaz C, Miniou P, Roblot N, Dierich A, Le Meur M, Melki J. Nuclear targeting defect of SMN lacking the C-terminus in a mouse model of spinal muscular atrophy. Human molecular genetics. 2000; 9:849–858. [PubMed: 10749994]

Gabanella F, Carissimi C, Usiello A, Pellizzoni L. The activity of the spinal muscular atrophy protein is regulated during development and cellular differentiation. Human molecular genetics. 2005; 14:3629–3642. [PubMed: 16236758]

Gavrilina TO, McGovern VL, Workman E, Crawford TO, Gogliotti RG, DiDonato CJ, Monani UR, Morris GE, Burghes AH. Neuronal SMN expression corrects spinal muscular atrophy in severe

SMA mice while muscle-specific SMN expression has no phenotypic effect. Human molecular genetics. 2008; 17:1063–1075. [PubMed: 18178576]

Habgood MD, Hopkins WG, Slack JR. Muscle size and motor unit survival in mice. J Physiol. 1984; 356:303–314. [PubMed: 6520789]

Hausmanowa-Petrusewicz I, Vrbova G. Spinal muscular atrophy: a delayed development hypothesis. Neuroreport. 2005; 16:657–661. [PubMed: 15858401]

Hayworth CR, Moody SE, Chodosh LA, Krieg P, Rimer M, Thompson WJ. Induction of neuregulin signaling in mouse schwann cells in vivo mimics responses to denervation. J Neurosci. 2006; 26:6873–6884. [PubMed: 16793894]

Heier CR, Satta R, Lutz C, DiDonato CJ. Arrhythmia and cardiac defects are a feature of spinal muscular atrophy model mice. Human molecular genetics. 2010; 19:3906–3918. [PubMed: 20693262]

Hsieh-Li HM, Chang JG, Jong YJ, Wu MH, Wang NM, Tsai CH, Li H. A mouse model for spinal muscular atrophy. Nature genetics. 2000; 24:66–70. [PubMed: 10615130]

Jablonka S, Schrank B, Kralewski M, Rossoll W, Sendtner M. Reduced survival motor neuron (Smn) gene dose in mice leads to motor neuron degeneration: an animal model for spinal muscular atrophy type III. Human molecular genetics. 2000; 9:341–346. [PubMed: 10655542]

Kang H, Tian L, Son YJ, Zuo Y, Procaccino D, Love F, Hayworth C, Trachtenberg J, Mikesh M, Sutton L, Ponomareva O, Mignone J, Enikolopov G, Rimer M, Thompson W. Regulation of the intermediate filament protein nestin at rodent neuromuscular junctions by innervation and activity. J Neurosci. 2007; 27:5948–5957. [PubMed: 17537965]

Kang H, Tian L, Thompson W. Terminal Schwann cells guide the reinnervation of muscle after nerve injury. Journal of neurocytology. 2003; 32:975–985. [PubMed: 15034280]

Kariya S, Park GH, Maeno-Hikichi Y, Leykekhman O, Lutz C, Arkovitz MS, Landmesser LT, Monani UR. Reduced SMN protein impairs maturation of the neuromuscular junctions in mouse models of spinal muscular atrophy. Human molecular genetics. 2008; 17:2552–2569. [PubMed: 18492800]

Kong L, Wang X, Choe DW, Polley M, Burnett BG, Bosch-Marce M, Griffin JW, Rich MM, Sumner CJ. Impaired synaptic vesicle release and immaturity of neuromuscular junctions in spinal muscular atrophy mice. J Neurosci. 2009; 29:842–851. [PubMed: 19158308]

Kummer TT, Misgeld T, Lichtman JW, Sanes JR. Nerve-independent formation of a topologically complex postsynaptic apparatus. The Journal of cell biology. 2004; 164:1077–1087. [PubMed: 15037598]

Le TT, Pham LT, Butchbach ME, Zhang HL, Monani UR, Coovert DD, Gavrilina TO, Xing L, Bassell GJ, Burghes AH. SMNDelta7, the major product of the centromeric survival motor neuron (SMN2) gene, extends survival in mice with spinal muscular atrophy and associates with full-length SMN. Human molecular genetics. 2005; 14:845–857. [PubMed: 15703193]

Lefebvre S, Burglen L, Reboullet S, Clermont O, Burlet P, Viollet L, Benichou B, Cruaud C, Millasseau P, Zeviani M, et al. Identification and characterization of a spinal muscular atrophy-determining gene. Cell. 1995; 80:155–165. [PubMed: 7813012]

Ling KK, Lin MY, Zingg B, Feng Z, Ko CP. Synaptic Defects in the Spinal and Neuromuscular Circuitry in a Mouse Model of Spinal Muscular Atrophy. PLoS One. 2010; 5:e15457. [PubMed: 21085654]

Liu H, Beauvais A, Baker AN, Tsilfidis C, Kothary R. Smn deficiency causes neuritogenesis and neurogenesis defects in the retinal neurons of a mouse model of Spinal Muscular Atrophy. Dev Neurobiol. 2010

Lorson CL, Androphy EJ. An exonic enhancer is required for inclusion of an essential exon in the SMA-determining gene SMN. Human molecular genetics. 2000; 9:259–265. [PubMed: 10607836]

Lorson CL, Hahnen E, Androphy EJ, Wirth B. A single nucleotide in the SMN gene regulates splicing and is responsible for spinal muscular atrophy. Proceedings of the National Academy of Sciences of the United States of America. 1999; 96:6307–6311. [PubMed: 10339583]

Love FM, Thompson WJ. Schwann cells proliferate at rat neuromuscular junctions during development and regeneration. J Neurosci. 1998; 18:9376–9385. [PubMed: 9801376]

Lu DX, Huang SK, Carlson BM. Electron microscopic study of long-term denervated rat skeletal muscle. Anat Rec. 1997; 248:355–365. [PubMed: 9214553]

Marques MJ, Conchello JA, Lichtman JW. From plaque to pretzel: fold formation and acetylcholine receptor loss at the developing neuromuscular junction. J Neurosci. 2000; 20:3663–3675. [PubMed: 10804208]

Martinez-Hernandez R, Soler-Botija C, Also E, Alias L, Caselles L, Gich I, Bernal S, Tizzano EF. The developmental pattern of myotubes in spinal muscular atrophy indicates prenatal delay of muscle maturation. J Neuropathol Exp Neurol. 2009; 68:474–481. [PubMed: 19525895]

McGovern VL, Gavrilina TO, Beattie CE, Burghes AH. Embryonic motor axon development in the severe SMA mouse. Human molecular genetics. 2008; 17:2900–2909. [PubMed: 18603534]

Mentis GZ, Blivis D, Liu W, Drobac E, Crowder ME, Kong L, Alvarez FJ, Sumner CJ, O'Donovan MJ. Early functional impairment of sensory-motor connectivity in a mouse model of spinal muscular atrophy. Neuron. 2011; 69:453–467. [PubMed: 21315257]

Misgeld T, Burgess RW, Lewis RM, Cunningham JM, Lichtman JW, Sanes JR. Roles of neurotransmitter in synapse formation: development of neuromuscular junctions lacking choline acetyltransferase. Neuron. 2002; 36:635–648. [PubMed: 12441053]

Monani UR. Spinal muscular atrophy: a deficiency in a ubiquitous protein; a motor neuron-specific disease. Neuron. 2005; 48:885–896. [PubMed: 16364894]

Murray LM, Comley LH, Thomson D, Parkinson N, Talbot K, Gillingwater TH. Selective vulnerability of motor neurons and dissociation of pre- and post-synaptic pathology at the neuromuscular junction in mouse models of spinal muscular atrophy. Human molecular genetics. 2008; 17:949–962. [PubMed: 18065780]

Nishimune H, Sanes JR, Carlson SS. A synaptic laminin-calcium channel interaction organizes active zones in motor nerve terminals. Nature. 2004; 432:580–587. [PubMed: 15577901]

Noakes PG, Gautam M, Mudd J, Sanes JR, Merlie JP. Aberrant differentiation of neuromuscular junctions in mice lacking s-laminin/laminin beta 2. Nature. 1995; 374:258–262. [PubMed: 7885444]

Park GH, Kariya S, Monani UR. Spinal muscular atrophy: new and emerging insights from model mice. Curr Neurol Neurosci Rep. 2010a; 10:108–117. [PubMed: 20425235]

Park GH, Maeno-Hikichi Y, Awano T, Landmesser LT, Monani UR. Reduced Survival of Motor Neuron (SMN) Protein in Motor Neuronal Progenitors Functions Cell Autonomously to Cause Spinal Muscular Atrophy in Model Mice Expressing the Human Centromeric (SMN2) Gene. J Neurosci. 2010b; 30:12005–12019. [PubMed: 20826664]

Parsons DW, McAndrew PE, Iannaccone ST, Mendell JR, Burghes AH, Prior TW. Intragenic telSMN mutations: frequency, distribution, evidence of a founder effect, and modification of the spinal muscular atrophy phenotype by cenSMN copy number. Am J Hum Genet. 1998; 63:1712–1723. [PubMed: 9837824]

Reddy LV, Koirala S, Sugiura Y, Herrera AA, Ko CP. Glial cells maintain synaptic structure and function and promote development of the neuromuscular junction in vivo. Neuron. 2003; 40:563–580. [PubMed: 14642280]

Rimer M, Mathiesen I, Lomo T, McMahan UJ. gamma-AChR/epsilon-AChR switch at agrin-induced postsynaptic-like apparatus in skeletal muscle. Mol Cell Neurosci. 1997; 9:254–263. [PubMed: 9268504]

Ruggiu M, Herbst R, Kim N, Jevsek M, Fak JJ, Mann MA, Fischbach G, Burden SJ, Darnell RB. Rescuing Z+ agrin splicing in Nova null mice restores synapse formation and unmasks a physiologic defect in motor neuron firing. Proceedings of the National Academy of Sciences of the United States of America. 2009; 106:3513–3518. [PubMed: 19221030]

Ruiz R, Casanas JJ, Torres-Benito L, Cano R, Tabares L. Altered intracellular Ca2+ homeostasis in nerve terminals of severe spinal muscular atrophy mice. J Neurosci. 2010; 30:849–857. [PubMed: 20089893]

Sasaki T, Mann K, Miner JH, Miosge N, Timpl R. Domain IV of mouse laminin beta1 and beta2 chains. Eur J Biochem. 2002; 269:431–442. [PubMed: 11856301]

Schrank B, Gotz R, Gunnersen JM, Ure JM, Toyka KV, Smith AG, Sendtner M. Inactivation of the survival motor neuron gene, a candidate gene for human spinal muscular atrophy, leads to massive cell death in early mouse embryos. Proceedings of the National Academy of Sciences of the United States of America. 1997; 94:9920–9925. [PubMed: 9275227]

Shababi M, Habibi J, Yang HT, Vale SM, Sewell WA, Lorson CL. Cardiac defects contribute to the pathology of spinal muscular atrophy models. Human molecular genetics. 2010; 19:4059–4071. [PubMed: 20696672]

Stevens L, Bastide B, Maurage CA, Dupont E, Montel V, Cieniewski-Bernard C, Cuisset JM, Vallee L, Mounier Y. Childhood spinal muscular atrophy induces alterations in contractile and regulatory protein isoform expressions. Neuropathol Appl Neurobiol. 2008; 34:659–670. [PubMed: 18363640]

Thompson W. Synapse elimination in neonatal rat muscle is sensitive to pattern of muscle use. Nature. 1983a; 302:614–616. [PubMed: 6835395]

Thompson W, Kuffler DP, Jansen JK. The effect of prolonged, reversible block of nerve impulses on the elimination of polyneuronal innervation of new-born rat skeletal muscle fibers. Neuroscience. 1979; 4:271–281. [PubMed: 424074]

Thompson WJ. Lack of segmental selectivity in elimination of synapses from soleus muscle of new-born rats. J Physiol. 1983b; 335:343–352. [PubMed: 6875882]

Vitte JM, Davoult B, Roblot N, Mayer M, Joshi V, Courageot S, Tronche F, Vadrot J, Moreau MH, Kemeny F, Melki J. Deletion of murine Smn exon 7 directed to liver leads to severe defect of liver development associated with iron overload. Am J Pathol. 2004; 165:1731–1741. [PubMed: 15509541]

Wishart TM, Huang JP, Murray LM, Lamont DJ, Mutsaers CA, Ross J, Geldsetzer P, Ansorge O, Talbot K, Parson SH, Gillingwater TH. SMN deficiency disrupts brain development in a mouse model of severe spinal muscular atrophy. Human molecular genetics. 2010; 19:4216–4228. [PubMed: 20705736]

Woodman SE, Sotgia F, Galbiati F, Minetti C, Lisanti MP. Caveolinopathies: mutations in caveolin-3 cause four distinct autosomal dominant muscle diseases. Neurology. 2004; 62:538–543. [PubMed: 14981167]

Zhang Z, Lotti F, Dittmar K, Younis I, Wan L, Kasim M, Dreyfuss G. SMN deficiency causes tissue-specific perturbations in the repertoire of snRNAs and widespread defects in splicing. Cell. 2008; 133:585–600. [PubMed: 18485868]

Zuo Y, Lubischer JL, Kang H, Tian L, Mikesh M, Marks A, Scofield VL, Maika S, Newman C, Krieg P, Thompson WJ. Fluorescent proteins expressed in mouse transgenic lines mark subsets of glia, neurons, macrophages, and dendritic cells for vital examination. J Neurosci. 2004; 24:10999–11009. [PubMed: 15590915]

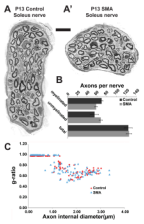

Fig. 1. No axon loss or change in myelination in nerve to the soleus muscle in SMAΔ7 mutant mice

EM cross-sections of soleus muscle nerves from P13 littermates, **A**. control nerve. **A'** mutant, SMA nerve. Sections were made proximal to the branch just outside the muscle. Scale bar = 10μm. **B**, Numbers of axons (myelinated, unmyelinated, and the total) found in 4 control and mutant soleus nerves were not statistically different. **C**, g-ratios (diameter of the axon/diameter of axon + sheath) plotted against the axon diameter illustrates axons have similar caliber and myelination. Unmyelinated axons were assigned a g-ratio of 1.

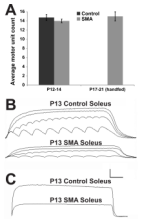

Figure 2. Nerve evoked contractions show mutant muscles are weak but provide no evidence of motor neuron death or deficits in neuromuscular transmission

A, The number of motor units counted in P12–14 control soleus muscles (14 ± 0.63) did not differ significantly from those in mutant littermates (14.75 ± 0.41, $p>0.36$), or P17 handfed mutant mice (15 ± 1, $p>0.84$). **B**, Isometric contractions of P13 control and mutant, SMAΔ7 soleus muscles to stimuli applied to the muscle nerve. A 1.5 sec duration train of stimuli was applied at frequencies of 5, 10, 20 and 60 Hz. Although the mutant muscle generated less than half the tension of the control, each stimulus applied generated a reliable muscle contraction. **C**, Response of control and mutant muscle to a 7.5 second duration tetanus at 60 Hz. Both muscles responded without obvious signs of fatigue or transmission failure. Calibration: 1g/100msec for A; 1g/1sec for B.

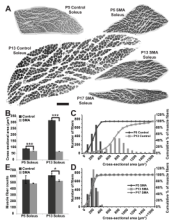

Figure 3. Reduction in SMN in soleus muscles of SMAΔ7 mice results in uniformly smaller and fewer muscle fibers

A, Cross-sections of control (P5 and P13) and mutant SMAΔ7 (P5, P13 and P17) soleus muscles stained with toludine blue. Scale bar = 100μm. **B**, Cross-sectional area of individual fibers in soleus. At P13, fibers are significantly smaller in mutant than control muscles. A difference in size was also apparent in the mutant at P5, although the magnitude of the difference was smaller than at P13. **C,D**, Distribution of fiber sizes shown as a histogram (left ordinate) and as a cumulative percentage (right ordinate). Reduction in fiber size occurs uniformly across fibers. Comparisons between controls and mutants at P5, P13 and P17 show that mutant fibers are uniformly reduced in cross-sectional area and fail to grow postnatally. **E**, Numbers of soleus fibers. At P13 mutant muscles have significantly fewer fibers than control muscles (ca. 15% fewer). However, at P5 the differences are not statistically significant. In each case 3 muscles of each type and age were examined; asterisks indicate statistical significance of comparisons (* $p<0.05$; *** $p<0.001$).

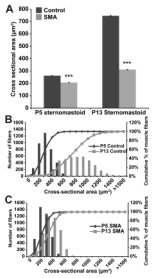

Figure 4. Defective postnatal growth of sternomastoid muscles in SMAΔ7 mice

A, Cross-sectional area of sternomastoid muscle fibers. As in soleus, mutant fibers were significantly smaller than age-matched control littermates at both P5 and P13. **B,C**, Distribution of fiber sizes as a histogram (left ordinate) and as a cumulative percentage (right ordinate). Growth of both control (**B**) and mutant (**C**) fibers is apparent in the right-shift in both graphs. The shift is much smaller for the mutant muscle fibers. The normal distribution of fiber sizes and smaller mean size suggest that fibers are uniformly reduced in size. In each case 3 muscles of each type and age were examined; asterisks indicate statistical significance of comparisons (*** $p < 0.001$).

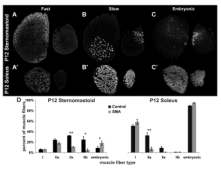

Figure 5. Expression of fast isoforms of myosin heavy chains is reduced in mutant SMAΔ7 muscles

A–C', Cryostat cross-sections immunostained with myosin heavy chain antibodies to identify fast, slow and embryonic types. P12 sternomastoid (top row) and soleus (bottom row) reacted with 3 of the antibodies used: **A, A'**, antibodies for fast myosin, 10F5 for IIb in A, N1.551 for IIa and neonatal myosin in A'; **B, B'**, A4.840 for slow myosin; **C, C',** F1.652 for embryonic myosin. Each pair of muscle sections shows the larger, control muscle and the smaller, mutant muscle (left and right in each pair, respectively). **D**, Fraction of muscle fibers of each type in mutant and control sternomastoid and soleus muscles. In the mutant muscles, fast type fibers are reduced, embryonic-expressing fibers are increased, while slow, type I fibers are unchanged. In each case 3 muscles of each type and age were examined; asterisks indicate statistical significance of comparisons (* $p<0.05$; ** $p<0.01$).

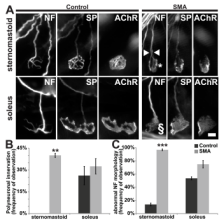

Figure 6. Morphology of mutant SMAΔ7 neuromuscular junctions suggests lack of synaptic maturation

The motor axons (neurofilament; NF), nerve terminal (synaptophysin, SP) and acetylcholine receptors (AChR) were fluorescently labeled. **A**, NMJs from P15 littermate control and mutant sternomastoid and soleus muscles. NMJs of mutant muscles appear immature and have accumulations of NF. While NF accumulations in most sternomastoid NMJs appeared “bulbous” (marked with asterisk), those of soleus synapses appeared “frayed” or “webbed” in appearance (marked with §). Scale bar = 10μm. **B**, Mutant sternomastoid muscles have a greater proportion of synapses that are polyneuronally innervated (white arrowhead in **A**, control, 0 ± 0%; mutant, 40 ± 1.4%; n=3, **p <0.01). In contrast, both control and mutant soleus NMJs have a large fraction of polyneuronal innervation (control, 26.1 ± 6.3%; mutant, 32.5 ± 5.3%; n=3, p >0.05). **C**, Accumulations of NF were found in nerve terminals of most mutant sternomastoid NMJs (control, 11.5 ± 1.4%; mutant, 96.8 ± 1.2%; n=3, ***p >0.001). Such accumulations were also found in a large proportion of both control and mutant soleus NMJs (control, 53.8 ± 2.6%; mutant, 76.1 ± 5.6%; p >0.05).

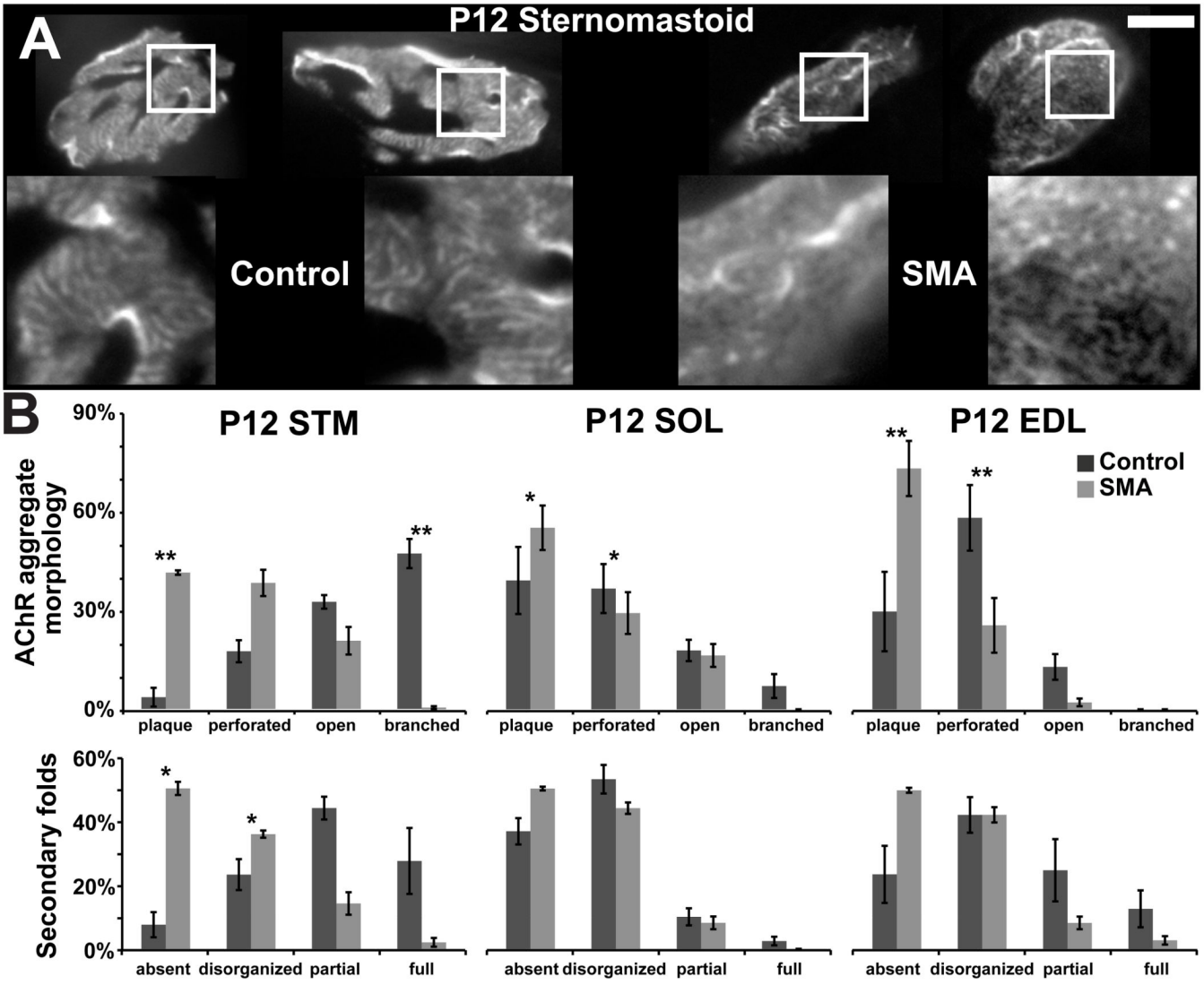

Figure 7. Impairment of postsynaptic maturation of SMAΔ7 mutants

A, Postsynaptic acetylcholine receptor (AChR) clusters of mutant sternomastoid muscle are less complex in comparison to those of control NMJs. Bright stripes of fluorescent α-bungarotoxin label, indicative of secondary postsynaptic folds (Marques et al., 2000), are less prominent or lacking in mutant compared to control (insets). Scale bar = 10μm. **B**, In P12 control sternomastoid, most AChR aggregates have evolved past the plaque stage into an open configuration, while only about 20% have reached this configuration in the mutant. The defects in AChR maturation are less evident in P12 mutant soleus and EDL; however, even control junctions of these muscles are immature at this stage of postnatal development. **C**, Mutant NMJs are also deficient in junctional folds. Junctional folds appear in parts or all of AChR aggregates in more than 70% of NMJs in P12 control sternomastoid. In contrast, a large majority of NMJs in P12 mutant sternomastoid lack or show patchy, short and/or disoriented stripes of AChR instead. While NMJs of mutant soleus and EDL muscles appear similar to those of mutant sternomastoid, the synapses in the control soleus and EDL muscles are equally immature. A minimum of 20 NMJs each from 3 muscles of each type at P12 were examined; asterisks indicate statistical significance of comparisons (* $p<0.05$; ** $p<0.01$)

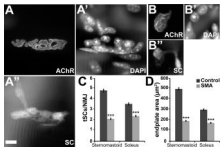

Figure 8. Fewer tSCs are associated with NMJs of mutant SMAΔ7 mice

A’’, **B’**, Identification of tSCs through transgenically expressed GFP label and nuclear labeling with DAPI **(A', B')** at NMJs of P13 control and mutant littermates. Postsynaptic AChR (**A**, **B**) were labeled with rhodamine-conjugated α-BTX. The number of tSCs was determined by comparing the GFP and the DAPI labels (indicated with asterisks). **C**, There is a significant reduction in the number of tSCs at mutant NMJs compared to controls in both sternomastoid and soleus muscles. **D**, SMAΔ7 mutant NMJs are smaller than in controls. (Sternomastoid: control, 512.5 ± 14.6 μm^2; mutant, 193.8 ± 6.8 μm^2; n≥149; soleus: control, 301.6 ± 10.8 μm^2; mutant, 175.4 ± 7.7 μm^2; n≥143, *** p<0.001). Scale bars = 10μm.

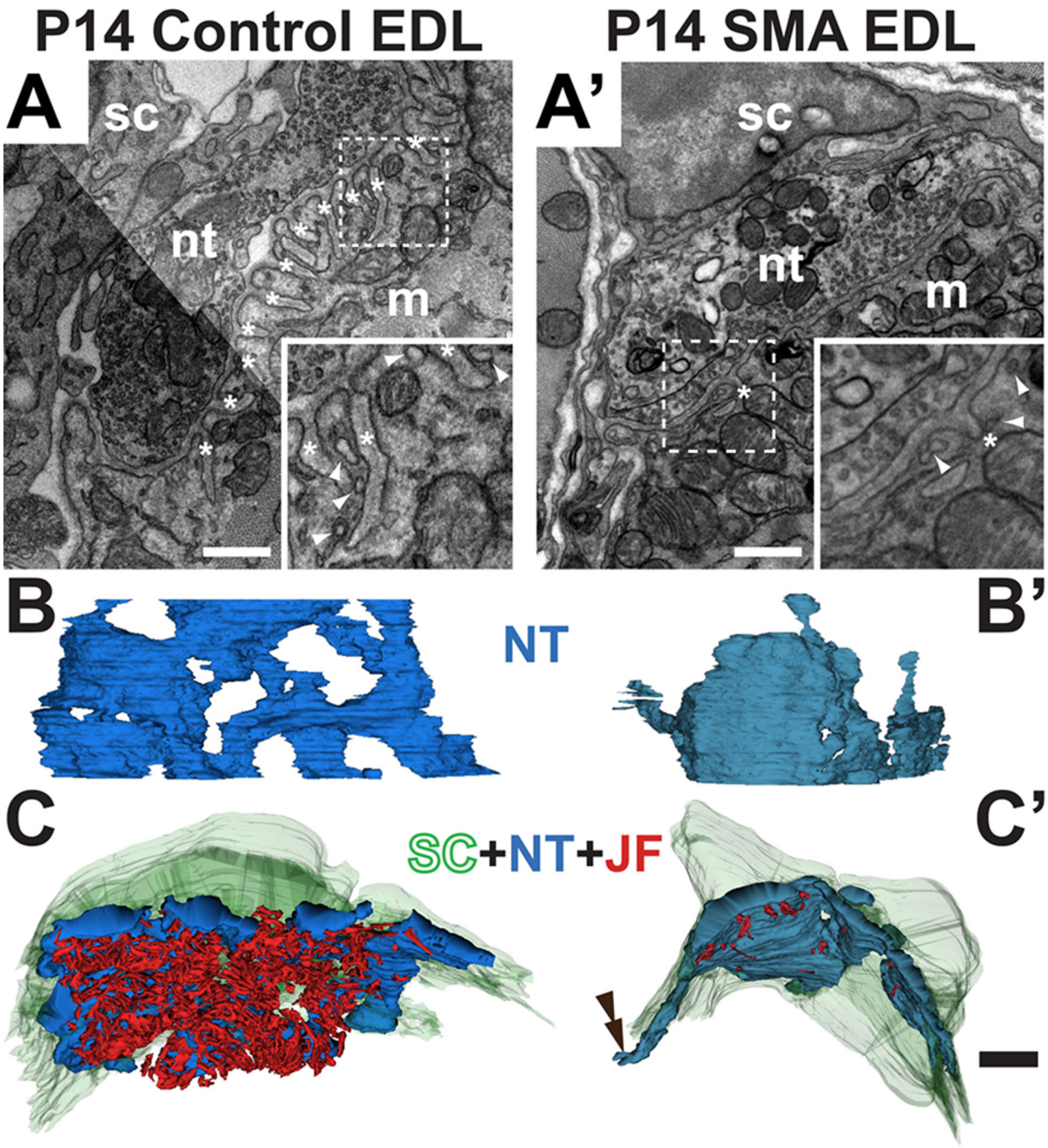

Figure 9. Ultrastructure of neuromuscular junctions shows structural changes in mutant junctions

EMs of control (**A**) and mutant (**A'**) P14 EDL NMJs. The three cellular components are indicated: m, postsynaptic muscle fiber, nt, presynaptic motor nerve terminal and sc, terminal Schwann cells. Junctional folds (labeled with *) are present in the control but largely absent in the mutant. Higher magnification images of the areas in dashed boxes (insets) illustrate fewer and shallower junctional folds (asterisks) as well as the caveolae-like structures (arrowheads). 3D reconstructions were rendered from serial EMs of control (**B**,**C**) and mutant (**B'**,**C'**). NMJs in the EDL muscle. The 3D reconstructions of the nerve terminal in B and B' were rotated so as to view the NMJs from the top. The mutant nerve terminal (in

blue) is less complex. The reconstructions in C and C' show the junctions viewed from inside the muscle fibers. The junctional folds, in red, are almost completely lacking in the mutant. The tSC (in green) incompletely covered the nerve terminal and its processes in the mutant (double arrowhead in **C'**). Scale bars in A–A' = 500nm and B–C' = 2μm.